Superatom Paramagnetism Enables Gold Nanocluster Heating in Applied Radiofrequency Fields

Ruthanne S. McCoy,[†] Sam Choi,[‡] George Collins,[‡] Bruce J. Ackerson,[§] and Christopher J. Ackerson[†,*]

[†]Department of Chemistry, Colorado State University, Fort Collins, Colorado 80521, United States, [‡]Department of Electrical Engineering, Colorado State University, Fort Collins, Colorado 80521, United States, and [§]Department of Physics, Oklahoma State University, Stillwater, Oklahoma 74078, United States

ABSTRACT The $Au_{102}(pMBA)_{44}$ nanocluster becomes a superatom paramagnet after chemical oxidation. Solutions of paramagnetic $Au_{102}(pMBA)_{44}$ heat in an oscillating magnetic field component of an RF field, but not in the electric component. Combined, these experiments suggest that paramagnetic $Au_{102}(pMBA)_{44}$ heats through interactions of spin magnetic moment with an external oscillating magnetic field. These results may clarify some current controversy regarding gold nanoparticle heating in radiofrequency fields.

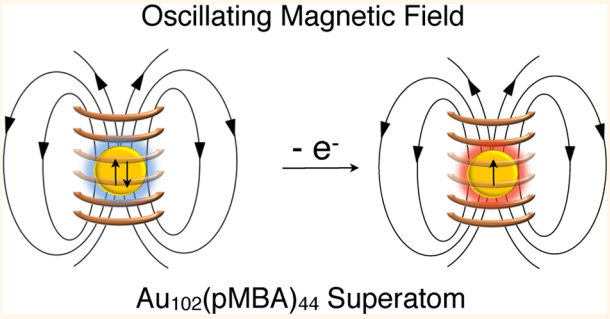

KEYWORDS: gold nanoparticles · hyperthermal therapy · radiofrequency · gold nanoclusters

Heating of metal nanoparticles by an applied radio frequency (RF) field attracts interest for potential applications in hyperthermal therapy,[1−4] biophysical manipulations,[5−7] and enhanced catalysis.[8] For heating of zerovalent metal nanoclusters and nanoparticles in RF fields, gold nanoparticles (AuNPs) are most widely studied. Reports of AuNP heating in an applied RF field generally attribute the observed thermal effect to a Joule-type heating, meaning the nanoparticles are considered to behave like very small pieces of bulk metal, and the subsequent confinement of conductive electrons provokes formation of eddy currents driven by electric fields surrounding the RF magnetic field (B-field) flux direction and contributing to resistive heating.[6−9]

The possibility that gold nanoparticles can heat by a Joule-type mechanism in an applied RF is disputed on both experimental[10] and theoretical[11] grounds. Experimental removal of excess salt ions from AuNP solutions is shown to essentially eliminate prior thermal effects attributed to AuNPs. Also, multiple theoretical investigations suggest AuNPs have only minor losses from eddy currents.[10,11] Furthermore, RF can cause Joule heating of ionic solutions, a phenomena used in pasteurization processes.[12] The present controversy is two-sided, however, with a recent theoretical study suggesting a conductive solution enhances the RF/nanoparticle interaction and is essentially required for nanoparticle heating.[13] A very recent report suggests that an electrophoretic oscillation mechanism of nanoparticle heating could account for AuNP heating in electric fields (E-fields) for 10 nm and smaller nanoparticles.[14]

The experiments that support RF heating were conducted in several different laboratories, whose experimental setups varied in AuNP size, AuNP dispersity, AuNP ligand shell composition, type of RF (transmitters emphasizing E-field, B-field, or both), frequency of RF, and power of RF. In the diversity of reports made, AuNP heating mechanisms other than Joule-type heating may also contribute and must be accounted for. In particular, mechanisms that consider the physical phenomena that arise with nanoscale noble metal nanoparticles may be important.

Herein we study the behavior of the $Au_{102}(pMBA)_{44}$ nanocluster[15,16] in multiple RF configurations and in multiple salt matrices in order to better unravel possible contributors to heating. Notably, the

* Address correspondence to ackerson@colostate.edu.

Received for review December 28, 2012 and accepted February 7, 2013.

Published online February 07, 2013
10.1021/nn306015c

$Au_{102}(pMBA)_{44}$ nanocluster is now well understood as a member of a magic number series of electronically closed shell gold nanocluster superatoms.[17] As prepared and observed in a crystal structure,[15] the superatom electron configuration is $(1S)^2$ $(1P)^6$ $(1D)^{10}$ $(2S)^2$ $(1F)^{14}$ $(2P)^6$ $(1G)^{18}$. Addition or removal of electrons from these superatomic orbitals may render the cluster a superatom paramagnet, as shown previously for $Au_{25}(SR)_{18}$.[18] The possible magnetic moment of AuNPs has not been previously considered as playing a role in their thermal properties in RF fields to our knowledge, as the magnetic properties of AuNPs are emergent and not fully understood.[19]

Magnetic nanoparticles such as superparamagnetic iron oxide nanoparticles (SPIONS), however, are well understood to respond to oscillating RF magnetic fields.[20,21] In this type of heating, the nanoparticle's interaction with an oscillating magnetic field results in Brownian (particle rotates within stationary solvent) and Néel (magnetic dipole rotates within the stationary particle) relaxations, which can both generate heat. Herein we show that $Au_{102}(pMBA)_{44}$ can be prepared as a paramagnet, and in an oscillating magnetic field such a paramagnet can both experimentally and theoretically heat above background temperatures in a variety of background matrixes discussed below. We also discuss how other previously reported experiments[6,7,22] may have contained unintentionally magnetic AuNP preparations in oscillating magnetic fields, partially accounting for the observed nanoparticle-dependent heating phenomena.

RESULTS

The total filling of the 58 electron 1G shell confers superatomic stability to $Au_{102}(pMBA)_{44}$.[15,17] Oxidation of the related $Au_{25}(SR)_{18}$ superatom nanocluster is shown to impart paramagnetism, resulting from unpaired electrons in the superatomic 1P shell.[18,23] Oxidation of the $Au_{102}(SR)_{44}$ cluster should also result in a superatom paramagnet, arising from unpaired superatom electron spins in the 1G superatom orbital.[17] Oxidation can in theory increase the superatomic spin state of the clusters to a maximum of $S = 9/2$, corresponding to the half-filling of the 1G HOMO.

Preliminary redox experiments with chemical[24] and electrochemical bulk electrolysis[25] oxidation approaches suggested $KMnO_4$ as an especially effective oxidant. We oxidized $Au_{102}(pMBA)_{44}$ with varying concentrations of $KMnO_4$, followed by removal of excess oxidant by precipitation followed by dialysis against distilled water. The resulting solutions contain only $Au_{102}(pMBA)_{44}$ and water, removing the potentially confounding factor of dissolved salts (*vide infra*). Polyacrylamide gel electrophoresis shows that $KMnO_4$ oxidation does not appear to alter the $Au_{102}(pMBA)_{44}$ nanocluster except in very high concentrations, where some aggregation is apparent (see Figure S1, Supporting Information). $Au_{102}(pMBA)_{44}$ oxidized with an optimized concentration of $KMnO_4$ was electrochemically and magnetically characterized. Electrochemical measurement of resting potentials of oxidized and control $Au_{102}(pMBA)_{44}$ were measured as 310 and 289 mV (*vs* saturated calomel electrode), indicating a successful oxidation of $Au_{102}(pMBA)_{44}$. Paramagnetism was determined by Evan's method[26,27] on both oxidized and control samples. The ^1H NMR spectrum for oxidized $Au_{102}(pMBA)_{44}$ shows splitting of the solvent peak (D_2O) into two distinct signals, indicating that the $Au_{102}(pMBA)_{44}$ has been rendered a paramagnet (Figure 1, bottom trace). As-syntheiszed $Au_{102}(pMBA)_{44}$ (control) shows no splitting of the solvent peak (Figure 1, top trace), as expected.

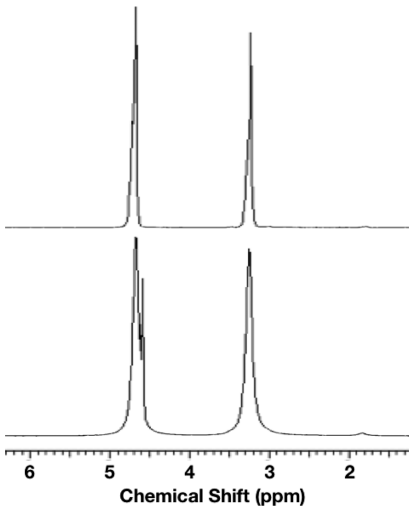

Figure 1. ^1H NMR of 100 μM $Au_{102}(pMBA)_{44}$ oxidized with 64× $KMnO_4$ (bottom trace) and 100 μM $Au_{102}(pMBA)_{44}$ as-synthesized control (top trace).

Magnetic iron oxide nanoparticles subjected to oscillating magnetic fields experience heating, and a substantial literature describing biomedical application of the RF hyperthermal properties of magnetic iron oxides (including ferromagnetic and superparamagnetic species) has emerged.[20] We sought to determine if paramagnetic $Au_{102}(pMBA)_{44}$ would similarly heat in an oscillating magnetic field.

Increasing amounts of oxidation may increase the paramagnetism of $Au_{102}(SR)_{44}$ to a maximum of $S = 9/2$, corresponding to a half-filled 1G superatom orbital. Figure 2 shows that oxidized (paramagnetic) $Au_{102}(pMBA)_{44}$ dissolved in distilled water and exposed to an oscillating magnetic field heats the solution, where the rate of heating depends on the oxidation state (and therefore superatomic spin state) of $Au_{102}(pMBA)_{44}$. For each successive oxidation attempt the initial rate of heating approximately doubles. For convenience the unregulated frequency of 13.56 MHz was used in this and successively described experiments.

We attribute the observed heating here to the magnetic moment of the nanoparticle interacting with

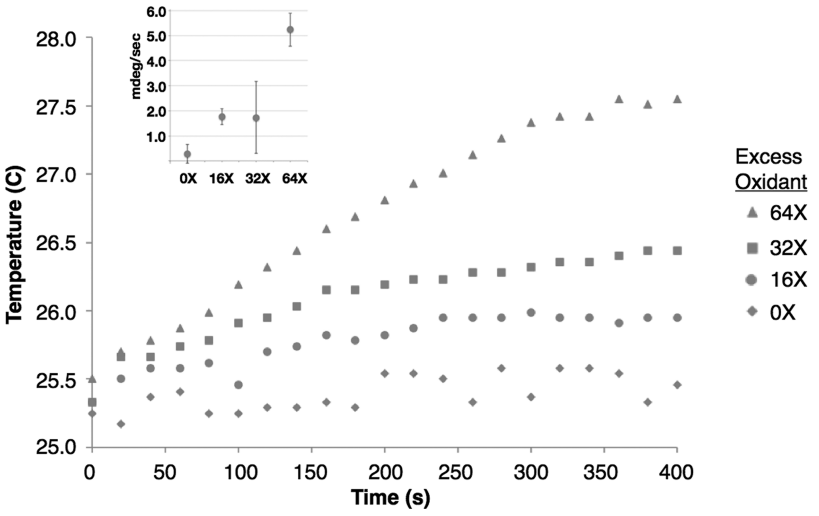

Figure 2. Time-dependent temperature of a solution of 100 μM $Au_{102}(pMBA)_{44}$ exposed to a 13.56 MHz 50 W magnetic field after the $Au_{102}(pMBA)_{44}$ is oxidized with the indicated molar excesses of $KMnO_4$. The bottom to top data points (diamonds, circles, squares, triangles) correspond to no oxidant, a 16× molar excess, a 32× molar excess, and a 64× molar excess of oxidant. Inset shows the average initial heating rate (millidegrees C/s) for each $KMnO_4$ excess attempted three times each, where the error bars show standard deviation of heating rate among the runs.

an external (oscillating) magnetic field. For magnetic iron oxides, heat generated in an oscillating magnetic field is attributed to a combination of Brownian and Néel relaxations. To gain insight into the mechanism for nanocluster heating observed here, we calculated the expected heating rate for the case of exclusively Brownian relaxation. For Brownian relaxation, the viscous drag of a nanoparticle dissolved in viscous solution produces the observed heating. This phenomena is well described by Rosensweig.[28]

The power production density from Rosensweig for monodisperse particle systems in the low-frequency, small magnetic field limit is given by

$$P = \frac{6\pi^2\mu_o{}^2H_d{}^2M_d{}^2V_HV_M}{(k_BT)^2}\eta\phi f^2 = \frac{6\pi^2B_o{}^2(M_dV)^2}{(k_BT)^2}\eta\phi f^2 \quad (1)$$

where μ_o is the permeability of free space, H_o is the magnetic field amplitude, M_d is the domain magnetization, V_m is the volume of the magnetized particle, V_H is the hydrodynamic volume, which is slightly larger than V_m due to adsorbed surfactant molecules (here V_m and V_H are set equal), η is the shear viscosity of the solvent, ϕ is the volume fraction of nanoparticles in suspension, f is the external magnetic field frequency, and k_BT is the thermal energy. The Brownian relaxation time in Rosensweig's theory is $\tau = (3\eta V_H)/(k_BT) \approx 10^{-7}$ s (eq 2, assumes 1.5 nm diameter particle), such that the frequency−relaxation time product is order unity. The field frequency is sufficiently slow that the particle follows the field.

The magnetic moment of the paramagnetic particles is estimated by M_dV_M in eq 1.The possible magnetic moment used in eq 1 for M_dV_M for $Au_{102}(pMBA)_{44}$ superatom paramagnets ranges from 9.28×10^{-24} (for S = 1/2) to 8.35×10^{-23} (for S = 9/2). Assuming an arbitrary total superatom electron spin S = 7/2, the total magnetic moment above is 6.49×10^{-23} J, and the resulting power density becomes

$$P = 1.45\mu_o{}^2H_o{}^2f^2\phi$$

(independent of nanoparticle radius)

This power density is the same order of magnitude as that estimated for Rosensweig's ferromagnetic particles of equivalent size. When the power density is divided by the product of the gold heat capacity and density, the rate of change of solution temperature is estimated as 0.22 mdeg/s. Since Brownian relaxation cannot account entirely for the observed heating rate, other heating mechanisms such as Néel relaxation or potentially unknown mechanisms must also contribute to the observed heating.

A solenoid generates primarily a magnetic field aligned along the central axis within the long and narrow radius electrode geometry and is commonly used as a magnetic field source in viscous heating of magnetic iron oxide nanoparticles,[20,29,30] as well as in some previous demonstrations of heating of AuNPs.[6] A time-dependent magnetic field also generates an E-field. To rule out this E-field as the source of observed heating, the bulk solution heating response of 100 μM $Au_{102}(pMBA)_{44}$ solutions was measured during RF irradiation in both a solenoid[6] (primarily B-field) and a copper-plate capacitor (capacitively coupled E-field).[8] Figure 3 shows that B-field irradiation provokes a much larger thermal response than E-field irradiation. As described in the experimental section, delivered power and frequency were the same in each case. While the differing geometries of the copper plates and solenoid may allow different amounts of flux at the sample, this probably cannot account for the difference seen in Figure 3. Also suggesting that the B- and not E-field dominates the heating process, we observe

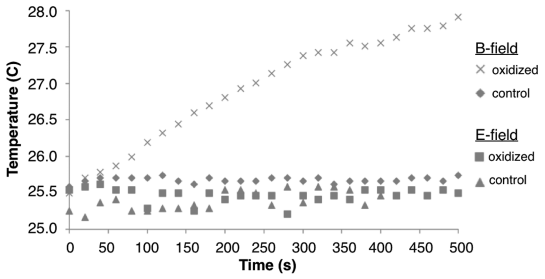

Figure 3. 100 μM $Au_{102}(pMBA)_{44}$ exposed to 13.56 MHz 50 W electromagnetic fields. Crosses and triangles represent oxidized and control $Au_{102}(pMBA)_{44}$, respectively, in a B-field. Squares and triangles represent oxidized and control $Au_{102}(pMBA)_{44}$, respectively, in the E-field.

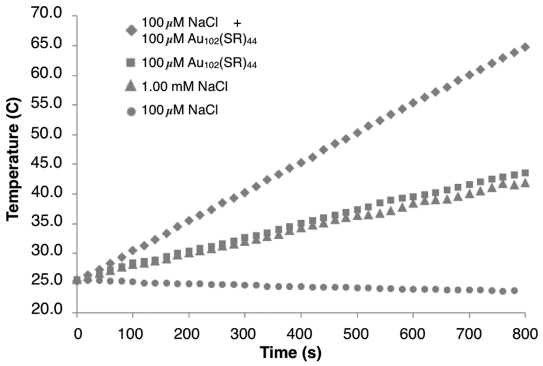

Figure 4. Bulk solution thermal response of 100 μM NaCl (circles), 1 mM NaCl (triangles), 100 μM $Au_{102}(pMBA)_{44}$ (squares), and 1 mM NaCl + 100 μM $Au_{102}(pMBA)_{44}$ (diamonds).

that samples in the center of a solenoid have a much higher rate of heating than those placed just outside the solenoid (Figure S2). The E-field generated by a solenoid depends on distance from the central axis, while the B-field is concentrated in the center of the coils (Figure S2). Taken collectively, the observation of paramagnetism after oxidation and the observation of high rates of heating in an oscillating magnetic field, but not electric field, suggest that the source of the observed heat is due, we judge, to the viscous drag of paramagnetic particles realigning their magnetic moment and reorienting to follow an oscillating RF magnetic field.

Ultimately we endeavor to apply the heating effects to manipulate biological systems, which contain other components that may interact with RF fields to provoke heat. Recent literature contains substantial controversy regarding the role of mobile ions in the heating of gold nanoparticle solutions, with the suggestion on one hand that Joule-type heating of conductive solutions and not the heating of AuNPs accounts for all of the observed heating, while on the other hand there is a suggestion that conductive solutions may be necessary for effective field penetration and interaction with nanoparticles.[13]

This controversy regarding the influence of dissolved salt ions[8,10,13] provoked a set of experiments to explore the empirical effect of NaCl concentrations wherein several concentrations of sodium chloride solution were compared with their $Au_{102}(pMBA)_{44}$ + salt analogues (Figure 4). In every case, the combination of nanoparticles and salt resulted in a greater heating response than either species alone, indicating a cooperative effect. This cooperative effect was most pronounced at 1 mM NaCl, as shown in Figure 4. The effect of other salt concentrations can be found in the Supporting Information (Figure S3).

DISCUSSION

Previous reports suggested that both primarily electric[8] and primarily magnetic[6] fields could provoke heating of gold nanoparticle solutions. Both forms of RF were initially hypothesized to provoke nanoparticles to heat through inductive effects.[6,8] Inductive heating of macroscopic metal samples in an oscillating electromagnetic field results from ohmic dissipation of eddy currents. For a 10 nm spherical metal nanoparticle, the electron mean free path is 100 times the particle radius; thus macroscopic resistance models have questionable validity, as highlighted by Geller[10] and Apell.[11]

Most previous reports of AuNP heating use AuNP targets of 5 nm diameter or larger, where superatom stabilization and potential superatomic paramagnetism is unlikely.[17,31] One notable previous report uses 1.4 nm diameter AuNPs,[6] where superatom paramagnetism may arise from oxidation by atmospheric O_2, a phenomena that was unknown at the time this paper was published. This report also used a solenoid as RF source; we suggest that the heating observed in this report may be due to serendipitously oxidized AuNP superatom paramagnets and not by the Joule mechanism originally suggested. Alternatively, we also cannot rule out that particles used in previous studies were serendipitous permanent magnets. Some reports suggest that AuNPs may be intrinsically magnetic as a function of size and surface nature,[32,33] although a recent comprehensive review demonstrates that measurements of magnetic properties of AuNPs are not consistent among different laboratories and often within the same lab, suggesting that AuNP magnetism is more complex than the current hypotheses.[19]

Since the heating of magnetic iron oxide nanoparticles in an oscillating magnetic field is well understood theoretically[28] and provides some precedent for our results, we make comparison to the known size effects in this theory. For 10 nm magnetic iron oxide nanoparticles the theory predicts experimental ferrofluid behavior, meaning that the particles will rotate to align with the magnetic field. For an iron oxide nanoparticle radius less than 7 nm, the Néel relaxation time becomes smaller than the viscous relaxation time. For these particles the magnetic moment follows the field without dragging the particle with it, so iron oxide

nanoparticles of the small size of $Au_{102}(pMBA)_{44}$ exhibit heating through Néel relaxations.

Could Brownian-type relaxations exclusively account for the observed heating? Density functional theory shows the electronic orbits are anisotropic as they extend into the ligand layer surrounding the gold core.[17] This may anchor the moment to the particle for sufficiently small energies. While we have no estimate for what these energies might be, the experimental results presented herein suggest that they are at least nonzero, allowing the moment alignment to drag the particle without slipping, producing the observed heat of viscous dissipation.

Much of the heating that we observe is modest and substantially less than reported in previous work on gold nanoparticle and magnetic iron oxide nanoparticle heating. The much smaller heating that we observe compared to other nanoparticle hyperthermia approaches may be due in part to our use of smaller power in the experiment (50 W compared to 600 W in other experiments) and also incomplete optimization of both cluster oxidation strategy and transmitter design. Preliminary calculations and data (data not shown) suggest, unsurprisingly, that RF frequency has a very strong impact on heating efficiency. The frequency and power used in this study were chosen for convenience and allowed demonstration of paramagnet heating in an oscillating magnetic field. Future work will optimize both RF generation and nanocluster magnetism, to allow better modulation of particle heating effects.

CONCLUSION

The $Au_{102}(pMBA)_{44}$ nanocluster can be made paramagnetic *via* chemical oxidation methods. Paramagnetism and oxidation were confirmed using Evan's NMR method and resting potential measurement. Salt-free paramagnetic $Au_{102}(pMBA)_{44}$ heats in an oscillating RF magnetic field, while a control sample of $Au_{102}(pMBA)_{44}$ does not. Furthermore, heating was observed only in transmitters that emphasize magnetic field and not in those emphasizing electric field. These results suggest that the mechanism of heat generation is through Brownian and Néel relaxations of nanoparticle magnetic moments, similar to that observed for magnetic iron oxide nanoparticles.

We addressed the controversy of salt heating[10,11] by systematically testing various sodium chloride concentrations in the absence and presence of $Au_{102}(pMBA)_{44}$. For nearly every pair, the combination of salt and nanoclusters resulted in markedly greater heating than either sample alone. Overall, we have clarified the thermal behavior of gold nanoparticles in radiofrequency fields.

METHODS

Synthesis of $Au_{102}(pMBA)_{44}$. Synthesis was performed as previously reported.[16] Briefly, 0.209 g of $HAuCl_4 \cdot 3H_2O$ was dissolved in 19 mL of nanopure water (18 mΩ), resulting in a 0.028 M solution. Then 0.292 g of *p*-mercaptobenzoic acid (pMBA) and 0.57 mL of 10 M NaOH were dissolved in 18.43 mL of nanopure water (0.1 M pMBA/0.3 M NaOH). A 250 mL beaker was charged with 51.5 mL of nanopure water and a stir bar. A 17.8 mL portion of the 0.028 M $HAuCl_4 \cdot 3H_2O$ solution was added to the beaker, followed immediately by the addition of 15.5 mL of the pMBA solution and 75 mL of methanol. The contents of the beaker were allowed to stir for 1 h; then 0.0207 g of $NaBH_4$ was added. The resulting black solution was allowed to stir for at least 17 h, then transferred to a 1000 mL Fleaker. Methanol was added until the total volume was ~800 mL, followed by the addition of 40 mL of 5 M NH_4OAc. The contents of the Fleaker were distributed into twenty 50 mL conical vials, which were centrifuged at 4000 rpm and 4 °C for 10 min. The supernatant was discarded, and 50 μL of 2 M NH_4OAc and 100 μL of nanopure water were added to each vial. The contents of the vial were then combined into two tubes, methanol was added to the 50 mL mark, and the tubes were centrifuged at 4000 rpm and 4 °C for 10 min. The resulting pellets were purified *via* fractional precipitation using 20%, 30%, 40%, and 50% methanol. The fractions were visualized using gel electrophoresis with an 18% polyacrylamide gel at 110 V for 90 min. To remove excess salts, the purified fraction was dialyzed using 3500 MWCO regenerated cellulose dialysis tubing (Fisherbrand part no. 21-152-9) into nanopure water.

Oxidation and Determination of Paramagnetism. Eight 2 mL samples in 50 mL conical vials containing 100 μM $Au_{102}(pMBA)_{44}$, 1X-64X $KMnO_4$, and 100 μL of pH 9.2 borate buffer were prepared. Following addition of $KMnO_4$ the samples were immediately precipitated by addition of 1 mL of 5 M NH_4OAc and methanol to the 50 mL mark, then were centrifuged at 4000 rpm and 4 °C for 10 min. The necessity to quickly remove the oxidant is to prevent changes in cluster size that can result from overexposure to a strong oxidant. The pink supernatant was discarded, and the samples were transferred to dialysis tubing. The samples were dialyzed for 24 h with a continuous-flow dialysis system consisting of a peristaltic pump (Bio Rad Econopump) that continuously pumped fresh nanopure water from a reservoir to a dialysis chamber to remove any remaining $KMnO_4$ and excess NH_4OAc.

Evan's method for determination of magnetic moment using NMR was performed using the 0× and 64× samples.[26] The samples were lyophilized and redissolved in 2 mL of D_2O, and a sealed capillary containing D_2O was placed inside the NMR tube. ^1H NMR spectra were collected using a Varian Inova 400 NMR spectrometer.

Resting potentials were measured for the 0× and 64× samples using a typical three-electrode setup consisting of a glassy carbon working electrode, platinum auxiliary electrode, and saturated calomel reference electrode. Measurements were done on a Bioanalytical Systems (BAS) 100B potentiostat.

Radiofrequency Generation and Temperature Measurement. A PM5192 variable function generator was used to produce a sinusoidal 13.56 MHz frequency and amplified using an SCCX100 signal amplifier. An oscilloscope was used to ensure that the identical sinusoidal signal of the correct frequency was employed during every experiment. For magnetic field generation, the signal amplifier was connected to a load matching box affixed with two tunable capacitors (Comet CV05C-500XE) to match 50 Ω resistance and a copper, hollow, water-cooled solenoid (10 cm in length with a radius of 4 cm and 15 turns). For electric field generation we employed a capacitive electrode configuration, where a load matching box of the same design was fitted with a capacitor made with 4 × 4 in. single-sided PCB board held about a half-inch apart with nylon spacers. In both studies the various solutions were placed within the electrode regions, where corresponding fields were maximum. Temperature measurements in samples were performed using a Neoptix Nomad NMD-A fiber optic temperature sensor. Samples were

contained in 5 or 7 mm NMR tubes containing 0.5 or 2 mL, respectively, and the fiber optic probe was positioned at the center of the sample depth for each measurement. During exposure to radiofrequency, the tube was positioned in the center of the coil (both longitudinally and radially) for consistency of field exposure and was centered in the capacitor as well. Temperature measurements are recorded every 20 seconds. The experiment is terminated when the solution reaches saturation, meaning a steady state has been reached and the temperature is no longer climbing, the solution begins to boil, or it is clear that the solution is cooling to equilibrate to the temperature of the cooled coil, indicating there is little or no response to the field.

Measurement of Magnetic Field Strength. A loop probe connected to an oscilloscope was inserted into the solenoid while operating at 13.56 MHz and 50 W. The amplitude of the sine wave was measured and used to calculate the magnetic field using the following approximate equation for B-fields on the solenoid axis:

$$B_0 = \frac{\mu_0 i_0 N}{L}$$

where μ_o is the permeability of free space, i_o is the current (calculated from the voltage read by the oscilloscope), N is the number of turns of the solenoid, and L is the length of the solenoid. The calculated magnetic field is 0.021 T.

Measurement of Electric Field Strength. Using a Tektronix P6015 oscilloscope probe, the voltage across the parallel plate capacitor was measured to be 1.64 kV and the electric field strength was calculated to be 1.1×10^5 V/m.

Conflict of Interest: The authors declare no competing financial interest.

Supporting Information Available: Additional figures showing gel images and heating with respect to solenoid geometry. This material is available free of charge *via* the Internet at http://pubs.acs.org.

Acknowledgment. The authors acknowledge financial support from Colorado State University. The authors thank Joseph Diverdi for useful conversations and Marcus Tofanelli for help in electrochemical measurements. This work was completed while C.J.A. was an American Federation for Aging Research New Investigator.

REFERENCES AND NOTES

1. Cardinal, J.; Klune, J. R.; Chory, E.; Jeyabalan, G.; Kanzius, J. S.; Nalesnik, M.; Geller, D. A. Noninvasive Radiofrequency Ablation of Cancer Targeted by Gold Nanoparticles. *Surgery* **2008**, *144*, 125–132.
2. Glazer, E. S.; Curley, S. A. Radiofrequency Field-Induced Thermal Cytotoxicity in Cancer Cells Treated with Fluorescent Nanoparticles. *Cancer* **2010**, *116*, 3285–3293.
3. Glazer, E. S.; Zhu, C.; Massey, K. L.; Thompson, C. S.; Kaluarachchi, W. D.; Hamir, A. N.; Curley, S. A. Noninvasive Radiofrequency Field Destruction of Pancreatic Adenocarcinoma Xenografts Treated with Targeted Gold Nanoparticles. *Clin. Cancer Res.* **2010**, *16*, 5712–5721.
4. Cherukuri, P.; Glazer, E. S.; Curley, S. A. Targeted Hyperthermia Using Metal Nanoparticles. *Adv. Drug Delivery Rev.* **2010**, *62*, 339–345.
5. Lal, S.; Clare, S. E.; Halas, N. J. Nanoshell-Enabled Photothermal Cancer Therapy: Impending Clinical Impact. *Acc. Chem. Res.* **2008**, *41*, 1842–1851.
6. Hamad-Schifferli, K.; Schwartz John, J.; Santos Aaron, T.; Zhang, S.; Jacobson Joseph, M. Remote Electronic Control of DNA Hybridization Through Inductive Coupling to an Attached Metal Nanocrystal Antenna. *Nature* **2002**, *415*, 152–155.
7. Kogan, M. J.; Bastus, N. G.; Amigo, R.; Grillo-Bosch, D.; Araya, E.; Turiel, A.; Labarta, A.; Giralt, E.; Puntes, V. F. Nanoparticle-Mediated Local and Remote Manipulation of Protein Aggregation. *Nano Lett.* **2006**, *6*, 110–115.
8. Moran, C. H.; Wainerdi, S. M.; Cherukuri, T. K.; Kittrell, C.; Wiley, B. J.; Nicholas, N. W.; Curley, S. A.; Kanzius, J. S.; Cherukuri, P. Size-Dependent Joule Heating of Gold Nanoparticles Using Capacitively Coupled Radiofrequency Fields. *Nano Res.* **2009**, *2*, 400–405.
9. Thomas, J. Particle Size Effect in Microwave-Enhanced Catalysis. *Catal. Lett.* **1997**, *49*, 137–141.
10. Li, D.; Jung, Y. S.; Tan, S.; Kim, H. K.; Chory, E.; Geller, D. A. Negligible Absorption of Radiofrequency Radiation by Colloidal Gold Nanoparticles. *J. Colloid Interface Sci.* **2011**, *358*, 47–53.
11. Hanson, G. W.; Monreal, R. C.; Apell, S. P. Electromagnetic Absorption Mechanisms in Metal Nanospheres: Bulk and Surface Effects in Radiofrequency-Terahertz Heating of Nanoparticles. *J. Appl. Phys.* **2011**, *109*, 124306.
12. Piyasena, P.; Dussault, C.; Koutchma, T.; Ramaswamy, H. S.; Awuah, G. B. Radio Frequency Heating of Foods: Principles, Applications and Related Properties—a Review. *Crit. Rev. Food Sci. Nutr.* **2003**, *43*, 587–606.
13. Pearce, J. A.; Cook, J. R. 2011 Annual International Conference of the IEEE Engineering in Medicine and Biology Society. *IEEE* **2011**, 5577–5580.
14. Corr, S. J.; Raoof, M.; Mackeyev, Y.; Phounsavath, S.; Cheney, M. A.; Cisneros, B. T.; Shur, M.; Gozin, M.; McNally, P. J.; Wilson, L. J.; *et al.* Citrate-Capped Gold Nanoparticle Electrophoretic Heat Production in Response to a Time-Varying Radio-Frequency Electric Field. *J. Phys. Chem. C* **2012**, *116*, 24380–24389.
15. Jadzinsky, P. D.; Calero, G.; Ackerson, C. J.; Bushnell, D. A.; Kornberg, R. D. Structure of a Thiol Monolayer-Protected Gold Nanoparticle at 1.1 a Resolution. *Science* **2007**, *318*, 430–433.
16. Heinecke, C. L.; Ni, T. W.; Malola, S.; Makinen, V.; Wong, O. A.; Häkkinen, H.; Ackerson, C. J. Structural and Theoretical Basis for Ligand Exchange on Thiolate Monolayer Protected Gold Nanoclusters. *J. Am. Chem. Soc.* **2012**, *134*, 13316–13322.
17. Walter, M.; Akola, J.; Lopez-Acevedo, O.; Jadzinsky, P. D.; Calero, G.; Ackerson, C. J.; Whetten, R. L.; Grönbeck, H.; Häkkinen, H. A Unified View of Ligand-Protected Gold Clusters as Superatom Complexes. *Proc. Natl. Acad. Sci. U. S.A.* **2008**, *105*, 9157–9162.
18. Zhu, M.; Aikens, C. M.; Hendrich, M. P.; Gupta, R.; Qian, H.; Schatz, G. C.; Jin, R. Reversible Switching of Magnetism in Thiolate-Protected Au25 Superatoms. *J. Am. Chem. Soc.* **2009**, *131*, 2490–2492.
19. Nealon, G. L.; Donnio, B.; Greget, R.; Kappler, J.-P.; Terazzi, E.; Gallani, J.-L. Magnetism in Gold Nanoparticles. *Nanoscale* **2012**, *4*, 5244–5258.
20. Kievit, F. M.; Zhang, M. Surface Engineering of Iron Oxide Nanoparticles for Targeted Cancer Therapy. *Acc. Chem. Res.* **2011**, *44*, 853–862.
21. Chan, K. W.; Chou, C. K. Use of Thermocouples in the Intense Fields of Ferromagnetic Implant Hyperthermia. *Int. J. Hyperthermia* **1993**, *9*, 831–848.
22. Araya, E.; Olmedo, I.; Bastus, N. G.; Guerrero, S.; Puntes, V. F.; Giralt, E.; Kogan, M. J. Gold Nanoparticles and Microwave Irradiation Inhibit Beta-Amyloid Amyloidogenesis. *Nanoscale Res. Lett.* **2008**, *3*, 435–443.
23. Venzo, A.; Antonello, S.; Gascón, J. A.; Guryanov, I.; Leapman, R. D.; Perera, N. V.; Sousa, A.; Zamuner, M.; Zanella, A.; Maran, F. Effect of the Charge State ($z = -1, 0, +1$) on the Nuclear Magnetic Resonance of Monodisperse $Au_{25}[S-(CH_2)_2Ph]_{18}^z$ Clusters. *Anal. Chem.* **2011**, *83*, 6355–6362.
24. Ackerson, C. J.; Jadzinsky, P. D.; Jensen, G. J.; Kornberg, R. D. Rigid, Specific, and Discrete Gold Nanoparticle/Antibody Conjugates. *J. Am. Chem. Soc.* **2006**, *128*, 2635–2640.
25. Tofanelli, M. A.; Ackerson, C. J. Superatom Electron Configuration Predicts Thermal Stability of $Au_{25}(SR)_{18}$ Nanoclusters. *J. Am. Chem. Soc.* **2012**, *134*, 16937–16940.
26. Evans, D. F. The Determination of the Paramagnetic Susceptibility of Substances in Solution by Nuclear Magnetic Resonance. *J. Chem. Soc.* **1959**, 2003–2005.
27. Auten, B. J.; Hahn, B. P.; Vijayaraghavan, G.; Stevenson, K. J.; Chandler, B. D. Preparation and Characterization of 3 nm Magnetic NiAu Nanoparticles. *J. Phys. Chem. C* **2008**, *112*, 5365–5372.

28. Rosensweig, R. E. Heating Magnetic Fluid with Alternating Magnetic Field. *J. Magn. Magn. Mater.* **2002**, *252*, 370–374.
29. Bae, K. H.; Park, M.; Do, M. J.; Lee, N.; Ryu, J. H.; Kim, G. W.; Kim, C.; Park, T. G.; Hyeon, T. Chitosan Oligosaccharide-Stabilized Ferrimagnetic Iron Oxide Nanocubes for Magnetically Modulated Cancer Hyperthermia. *ACS Nano* **2012**, *6*, 5266–5273.
30. Tassa, C.; Shaw, S. Y.; Weissleder, R. Dextran-Coated Iron Oxide Nanoparticles: a Versatile Platform for Targeted Molecular Imaging, Molecular Diagnostics, and Therapy. *Acc. Chem. Res.* **2011**, *44*, 842–852.
31. Wong, O. A.; Heinecke, C. L.; Simone, A. R.; Whetten, R. L.; Ackerson, C. J. Ligand Symmetry-Equivalence on Thiolate Protected Gold Nanoclusters Determined by NMR Spectroscopy. *Nanoscale* **2012**, *4*, 4099–4102.
32. Crespo, P.; Litran, R.; Rojas, T.; Multigner, M.; la Fuente, de, J.; Sanchez-Lopez, J.; Garcia, M.; Hernando, A.; Penades, S.; Fernandez, A. Permanent Magnetism, Magnetic Anisotropy, and Hysteresis of Thiol-Capped Gold Nanoparticles. *Phys. Rev. Lett.* **2004**, *93*, 087204.
33. Negishi, Y.; Tsunoyama, H.; Suzuki, M.; Kawamura, N.; Matsushita, M. M.; Maruyama, K.; Sugawara, T.; Yokoyama, T.; Tsukuda, T. X-ray Magnetic Circular Dichroism of Size-Selected, Thiolated Gold Clusters. *J. Am. Chem. Soc.* **2006**, *128*, 12034–12035.